Biophysical Journal, Volume *111*

Supplemental Information

Segmentation of 3D Trajectories Acquired by TSUNAMI Microscope: An Application to EGFR Trafficking

Yen-Liang Liu, Evan P. Perillo, Cong Liu, Peter Yu, Chao-Kai Chou, Mien-Chie Hung, Andrew K. Dunn, and Hsin-Chih Yeh

Supplementary Information

Segmentation of 3D Trajectories Acquired by TSUNAMI Microscope: An Application to EGFR Trafficking

Yen-Liang Liu[1], Evan P. Perillo[1], Cong Liu[1], Peter Yu[1], Chao-Kai Chou[2, 3], Mien-Chie Hung[2,3], Andrew K. Dunn[1] & Hsin-Chih Yeh[1]*

[1]Department of Biomedical Engineering, University of Texas at Austin, Austin, TX, USA; [2]Department of Molecular and Cellular Oncology, The University of Texas MD Anderson Cancer Center, Houston, TX, USA; [3]Center for Molecular Medicine and Graduate Institute of Cancer Biology, China Medical University, Taichung, Taiwan.

Content

Monte Carlo simulations of EGFR movement in live cells

We performed five different sets of Monte Carlo simulations to generate 3D trajectories *in silico* that mimicked (*i*) Brownian diffusion; (*ii*) corralled diffusion in confinements with impermeable boundaries; (*iii*) hop diffusion in confinements with permeable boundaries; (*iv*) cage diffusion in vesicles that themselves can diffuse; and (*v*) directed motion along linear tracks with lateral diffusivity. Brownian diffusion simulations were performed by generating a set of random displacements ($\Delta x, \Delta y, \Delta z$) at each time step. These displacements followed a normal distribution with the following standard deviation:

$$\sigma_{x,y,z} = (2D_{Brn}\,\Delta t)^{1/2}$$

where D_{Brn} is the given diffusion coefficient and Δt is the time step used in simulation. In our simulation, D_{Brn} ranged from 0.01 to 0.16 μm/s^2, which were close to the reported EGFR diffusivities (tagged with a nanoparticle and diffusing on the plasma membrane) (1-3). Corralled diffusion simulations were performed by having a particle freely diffuse in cubes (D_{micro}) with impermeable boundaries and linear sizes (L) of 25, 50, 100 and 200 nm. If particles attempt to penetrate the boundaries of any dimension, the random displacement in the specific dimension(s) will be zero at this time step. Hop diffusion simulations were performed by having a particle freely diffuse in cubes (D_{micro}) with the same linear sizes, but now cubes had permeable boundaries (probability of penetration per attempt P = 0.01). The selected cube sizes were close to the 40 to 300 nm linear compartment sizes reported by other groups (2, 4, 5). Cage diffusion simulations were performed by having a particle freely diffuse within vesicles with impermeable boundaries and diameters (⌀) of 25, 50, 100 and 200 nm. Vesicles themselves were also diffusing ($D_{vesicle}$). These simulations were performed with D_{micro} = 0.5 μm^2/s and $D_{vesicle}$ = 0.01 μm^2/s. Corralled, hop and cage diffusion are all considered as "confined diffusion". Directed diffusion simulations were performed along linear tracks with active transport speeds (V) and lateral diffusivities ($D_{lateral}$). The movement of an internalized early endosome is mostly assisted by molecular motors on microtubules, therefore showing a characteristic transport speed (V) about 1 μm/s (6, 7) with lateral diffusivity ($D_{lateral}$) around 0.003 μm^2/s (8). The directed diffusion simulations were performed with V = 0.5 and 1 μm/s, and $D_{lateral}$ = 0.0025, 0.005, 0.01 and 0.02 μm^2/s. All simulations were performed with the time step (Δt) of 2.5 ms.

Simulation and experiment statements

For **Figures S5** and **S8**, the Monte Carlo simulations were performed for 10 s per run and 100 runs per case. White Gaussian noise type of tracking error (μ_{error} = 0 and σ_{error} = 15 nm) was added to the Monte Carlo simulation generated trajectories before being analyzed by the developed algorithm. The rolling window of 1.6 s (w) and the sliding time step of 0.1 s (Δs) were used to analyze the stimulated trajectories (time step Δt = 2.5 ms).

For **Figures S4**, **S9, S10-13**, the simulated movement experiments (SME) were performed for 30 s per run and 10 runs per case. ⌀200 nm fluorescent beads (F-8810, Thermo Fisher Scientific) were embedded in 1.3% agarose within chambered coverglass at 20 pM. Monte-Carlo-simulation-generated trajectories (without the white noise error) were used to command the movement of the xyz piezo stage every 2.5 ms. Although there were finite differences between the Monte-Carlo-simulation-generated trajectory and the actual trajectory that the stage performed (output from the capacitance sensors in the xyz piezo stage), we conveniently called both these two trajectories the prescribed trajectories. The xyz piezo stage moved once every 2.5 ms and the capacitance sensor recorded the piezo stage voltages every 1 ms, while the integration period of TSUNAMI

microscope was 5 ms. The rolling window of 1.6 s (w) and the sliding time step of 0.1 s (Δs) were used to analyze the experimental trajectories (time step Δt = 5 ms).

Data processing

All data processing was performed in MATLAB (Mathworks). Saved in a binary format, the trajectory raw data contained photon counts and voltage outputs from the actuators (i.e. the xy scanning galvo mirrors (6125H, Cambridge Technology) and the objective z-piezo stage (P-726 PIFOC, PI)) at each time point. Conversion of voltage outputs to particle xyz positions was carried out by multiplying a gain factor for each axis. Trajectories were plotted by simply connecting particle positions of consecutive time points. The particle-trajectory-derived diffusivities of membrane proteins were previously shown to have a broad distribution (9, 10) due to membrane heterogeneity (9). Rather than normal distribution, lognormal distribution was often used to describe the broad distribution of particle-trajectory-derived diffusivity (9, 10). We also observed this trend of lognormal distribution for our particle-trajectory-derived D_{Brn}, D_{micro}, D_{macro}, D_0, V, V_i and L values. The histograms of log$D$, log$V$ and log$L$ were fitted with a Gaussian mixture model (MATLAB, MathWorks). The fitted arithmetic means (μ) and standard deviations (σ) of log$D$, Log$V$, *and* log$L$ were converted to arithmetic means and standard deviations in a linear scale (11).

Optimization of thresholds used for classification

The calculations of these three classification parameters, the scaling component (α) of MSD curves, the directional persistence ($\Delta\phi$), and the confinement index (Λ) were shown in **Figure S3**. The schematic in **Figure S3** also demonstrate the difference of classification parameters in various motional modes.

Table S1 summarized the threshold optimization for the segmentation and classification algorithm. To find out the optimal rolling window length for our segmentation analysis, we calculated scaling exponents α and directional persistence $\Delta\phi$ of directed diffusion SME trajectories (**Figure S4**). The scaling exponent and directional persistence are functions of width of rolling window (w), lateral diffusion coefficient (D_{Lat}), and speed of active transport (V). To set the thresholds to differentiate directed diffusion from passive motion, SME with a set of various w, D_{Lat} , and V were tested and evaluated to determine the optimal w and the thresholds of α and $\Delta\phi$ (**Figure S4**). The simulation parameters (D_{Lat} and V) were referred to values observed in live cells. The D_{Lat} of an endosome conducting active transport in live cell is usually less than 0.01 $\mu m^2/s$ (12, 13), and the V ranges from 0.3 to 2 μm/s (8, 13, 14).

The confinement levels were calibrated with Monte Carlo simulations of Brownian diffusion, confined diffusion, and immobilization (**Figure S5**). The Λ_{Brn} would be a constant under the assumption that D_{max} equals to D_{Brn} (15). To analyze tracking trajectories, the D_{max} need to be derived from experimental trajectories. The Λ_{Im} is determined by the detection limit of tracking system (tracking error (σ_{error}), **Figure S6**) (16). The confinement levels of these three motional modes were defined by Λ_{Brn} and Λ_{Im}. The test of differentiating confined diffusion from Brownian diffusion were conduct in SME (**Figure S7**).

Flow chart for threshold optimiaztion

- Thresholding of α, $\Delta\phi$, and w

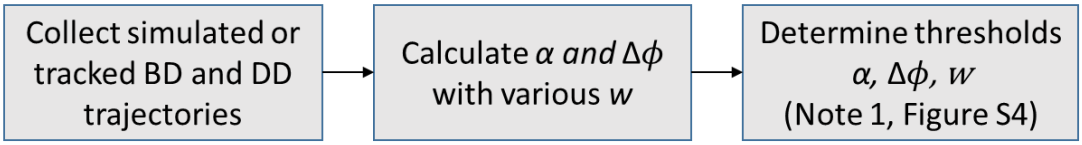

- Thresholding of Λ_{Brn}, Λ_{con}, and Λ_{Im}

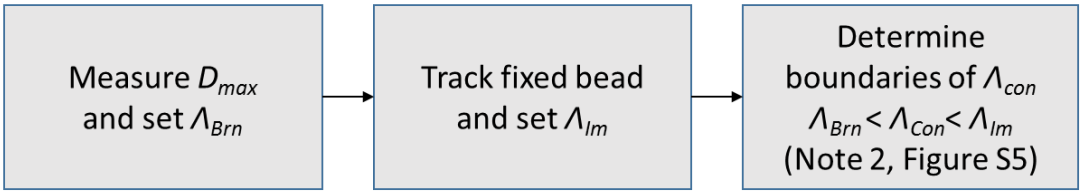

Table S1 | Threshold optimization

Classification parameters	Calibration models (Monte Carlo Simulation)	Threshold values	Note
$\alpha = f_1(w, D_{Lat}, V)$ $\Delta\phi = f_2(w, D_{Lat}, V)$	**Directed diffusion (DD)** D_{Lat} = 0.0025-0.02 μm²/s V = 0.5, 1 μm/s w = 0.06-1.6 s σ_{error}= 15 nm	• Directed diffuison $\begin{cases} \alpha > 1.4 \\ \Delta\phi < 0.1 \end{cases}$ • Passive motion $\begin{cases} \alpha < 1.4 \\ \Delta\phi > 0.1 \end{cases}$ • w = 1.6 s	**1.1** The thresholds of w, α, and $\Delta\phi$ were determined by the SME results (Figure S4). **1.2** If the D_{Lat} of directed diffusion is greater than 0.02 μm²/s or V is slower than 0.5 μm/s, the w might need to be increased to identify directed diffusion.
$\Lambda = f_3(w, D, D_{max}, L)$	**Brownian diffusion (BD)** D = 0.08 μm²/s **Confined diffusion (CD)** D = 0.08 μm²/s L = 25-1000 nm **Immobilization (IM)** σ_{error}= 15 nm	• BD: $\Lambda \leq \Lambda_{Brn}$ • CD: $\Lambda_{Brn} < \Lambda < \Lambda_{Im}$ • IM: $\Lambda \geq \Lambda_{Im}$ • Λ_{Brn} = 14.32 • Λ_{Im} = 677.59 • w = 1.6 s	**2.1** D_{max} is the cutoff of top 5% of diffusion coefficients derived from all trajectories, and D_{max} is assumed to be the D_{Brn} in live cells. The Λ of Brownian diffusion would be independent of w. **2.2** The Λ_{Brn} is defined as the cutoff of top 5% of Λ derived from Brownian diffusion. The Λ_{Brn} will be a constant if D_{max} equals to D_{Brn}. **2.3** The Λ_{Im} is determined by tracking error and defined as the cutoff of bottom 5% of Λ derived from immobilization trajectories.

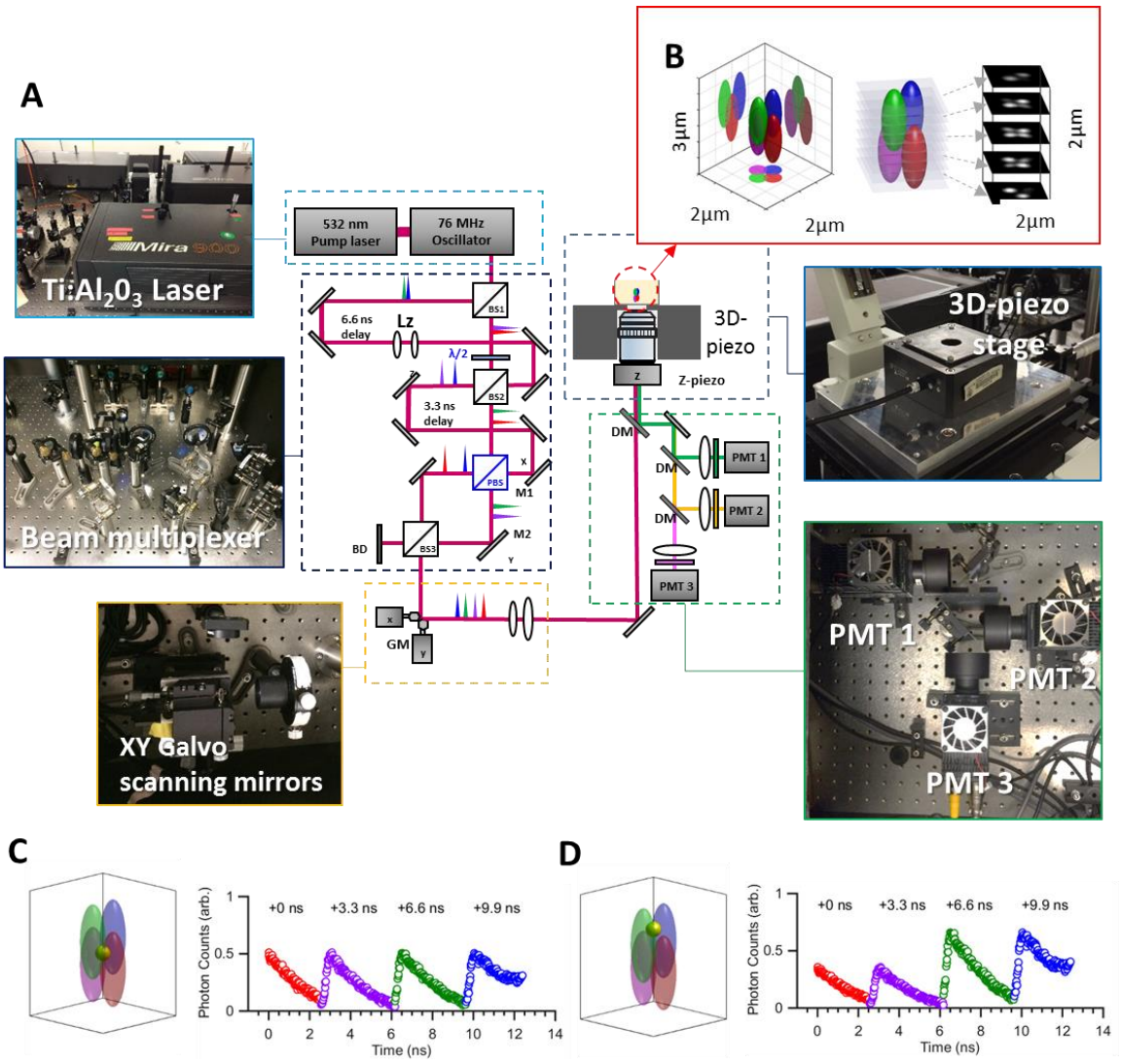

Figure S1 | TSUNAMI microscope setup (including the independent xyz piezo stage for SME) **(A)** The schematic and photograph of the Schematics of TSUNAMI (Tracking of Single particles Using Nonlinear And Multiplexed Illumination) 3D tracking microscope (17). The pulsed laser (76 MHz from a Ti-sapphire laser) is separated into four beams, which are delayed by 3.3 ns each and focused through a high-N.A. objective, generating four barely overlapped two-photon excitation volumes (colored oval balls in **(B)).** Using time-correlated-single-photon counting (TCSPC) detection, each detected photon attributed from an individual excitation volume is assigned to a specific time gated fluorescence decay histogram. An offset of the particle from the tetrahedron center can be estimated from the normalized photon count differences in the four time gates. As described in the paper, an independent xyz piezo stage (P-733K130, PI) is added to the system for SME, which allows us to quantify the tracking error of TSUNAMI microscope. *Lz*: lens set for z-offset control; *BS*: beam splitter; *λ/2*: half-wave plate; *PBS*: polarizing beam splitter; *DM*: dichroic mirror; *BD*: beam dump; *GM*: galvo mirrors; *M*: steering mirrors; *PMT*: photomultiplier tube. **(C)** When the particle (the golden sphere) sits right at the center of the illumination tetrahedron, photon counts are about equal in the four histograms. **(D)** The photon counts in the four histograms fluctuate according to the position of particle in the illumination tetrahedron.

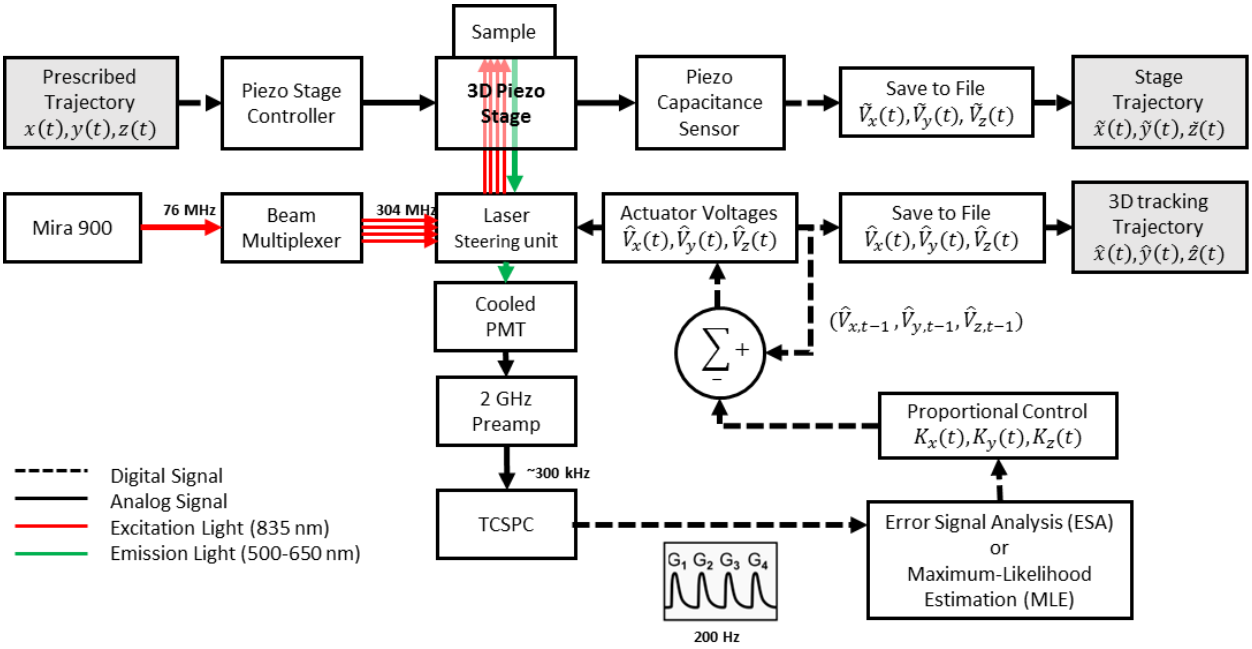

Figure S2 | TSUNAMI feed-back control schematic (including scheme for SME)

A Control Schematic demonstrating system level interaction, feedback control loop, and prescribed motion driven by an xyz piezo stage. The 835 nm excitation ray generated by a Ti:Al_2O_3 laser (Mira 900, Coherent) at 76 MHz repetition rate passes through the beam multiplexer and creates an illumination tetrahedron onto the sample. The sample is driven by an independent xyz piezo stage with a prescribed trajectory ($x(t), y(t), z(t)$). The piezo controller can simultaneously generate defined motion and record the corresponding motion profile which is then converted to a stage trajectory ($\tilde{x}(t), \tilde{y}(t), \tilde{z}(t)$). Fluorescence is detected by a cooled low dark count PMT (H7422PA-40, Hamamatsu Corp.) and amplified with a 2 GHz cutoff bandwidth preamplifier (HFAC-26, Becker and Hickl GmbH). The amplified signal is then measured and correlated to the reference clock of the Ti:Al_2O_3 laser with a TCSPC board (SPC-150, Becker and Hickl GmbH). Every 1-20 ms a photon histogram is sampled from the TCSPC module and processed in the software loop run in LabVIEW (National Instruments). The tracking algorithm employs a proportional control to convert the error signals to new stage positions. Furthermore, Liu and coworkers have demonstrated that the z-tracking accuracy can be significantly increased using maximum likelihood estimations (MLE) (18). New voltages are sent out through a DAQ (PCIe-6353, National Instruments) to their respective actuators, galvo mirrors for X and Y, piezo objective stage for Z. The saved voltages are converted to a 3D tracking trajectory ($\hat{x}(t), \hat{y}(t), \hat{z}(t)$).

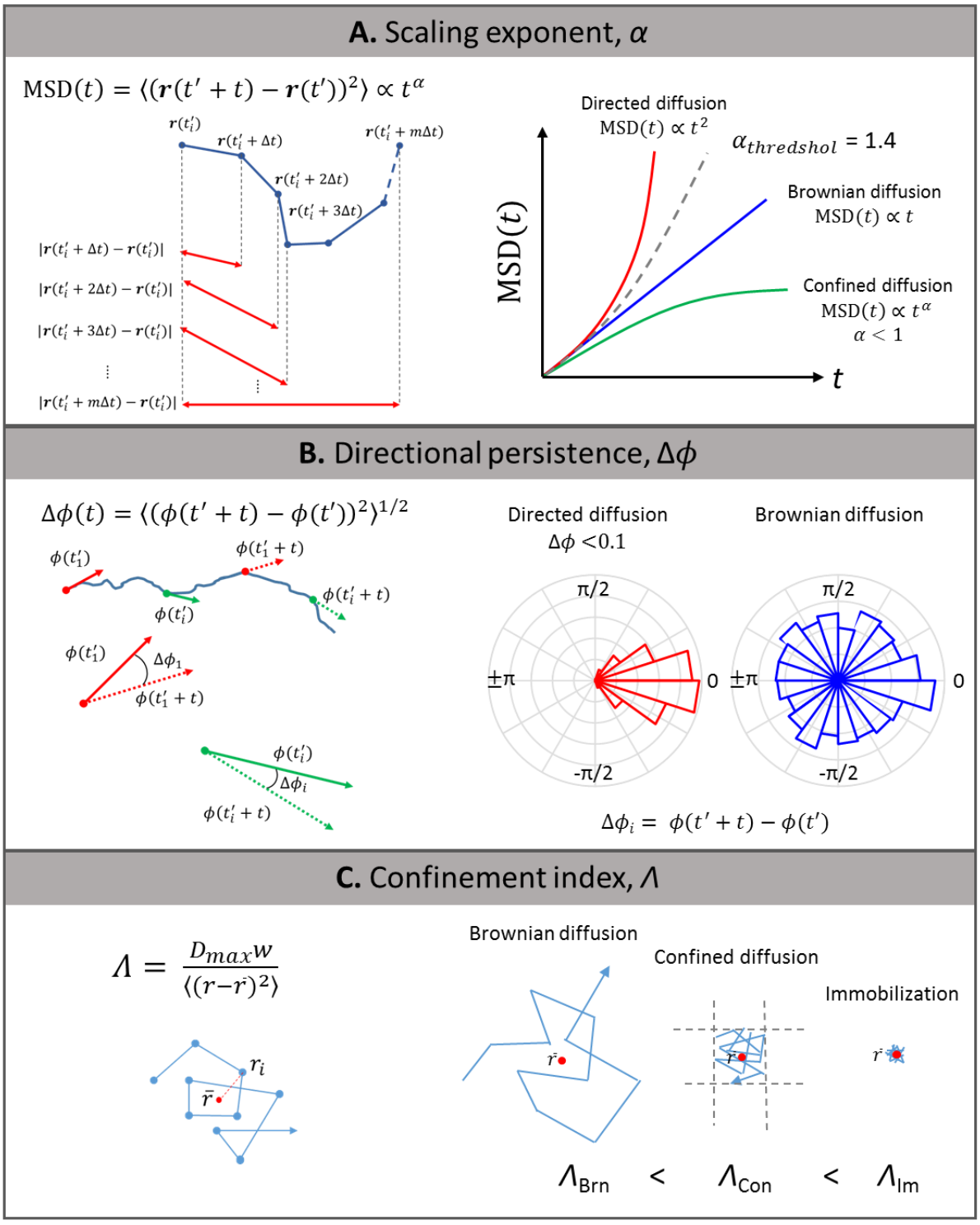

Figure S3 | Parameters for trajectory classification and segmentation

(A) Schematics show the calculation of a MSD curve and the representative MSD curves of directed diffusion, Brownian diffusion, and confined diffusion. **(B)** Schematics demonstrate the calculation of the directional persistence and the comparison of directional angles of directional diffusion and Brownian diffusion. **(C)** Calculation of confinement index and the indices derived from there three types of diffusions.

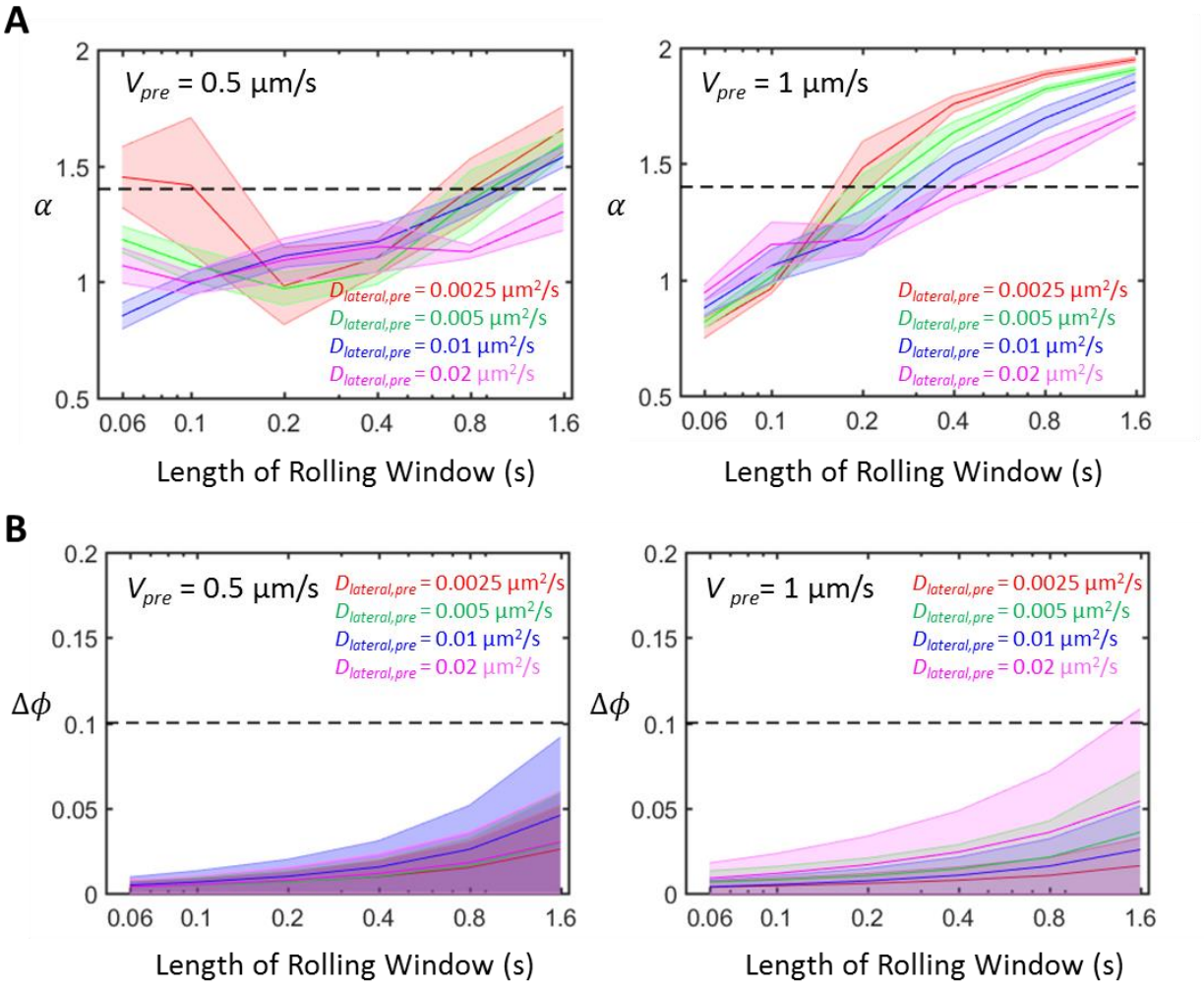

Figure S4 | Selecting threshold of the scaling exponent (α), directional persistence ($\Delta\phi$) and length of the rolling window (w) for directed diffusion detection (SME results)

Directed motions with various lateral diffusion coefficients (0.0025, 0.005, 0.01, or 0.02 μm²/s) and velocities (0.5 or 1 μm/s) were conducted in SME. The track duration for each trajectory is 10 seconds, and the time step is 2.5 ms. The α and $\Delta\phi$ values were derived from the MSD curves of the SME trajectoires. **(A)** The results demonstrate the diffusion would conceal the identification of directed motions, and the accuray of the algorithm depends on the window sizeWe set the threshold of identifying directed motion to be 1.4, because the active transport along microtubules exhibits α values of range from 1.4 to 2 in the cytosol (8). The time window was chosen as 1.6 s to achieve sufficient discrimination of active transport states. **(B)** Considering the time window of 1.6 s chosen to calculate α values, we set the threshold of $\Delta\phi$ values to be 0.1. Error bars (represented by color ribbons) show standard deviations of 10 runs.

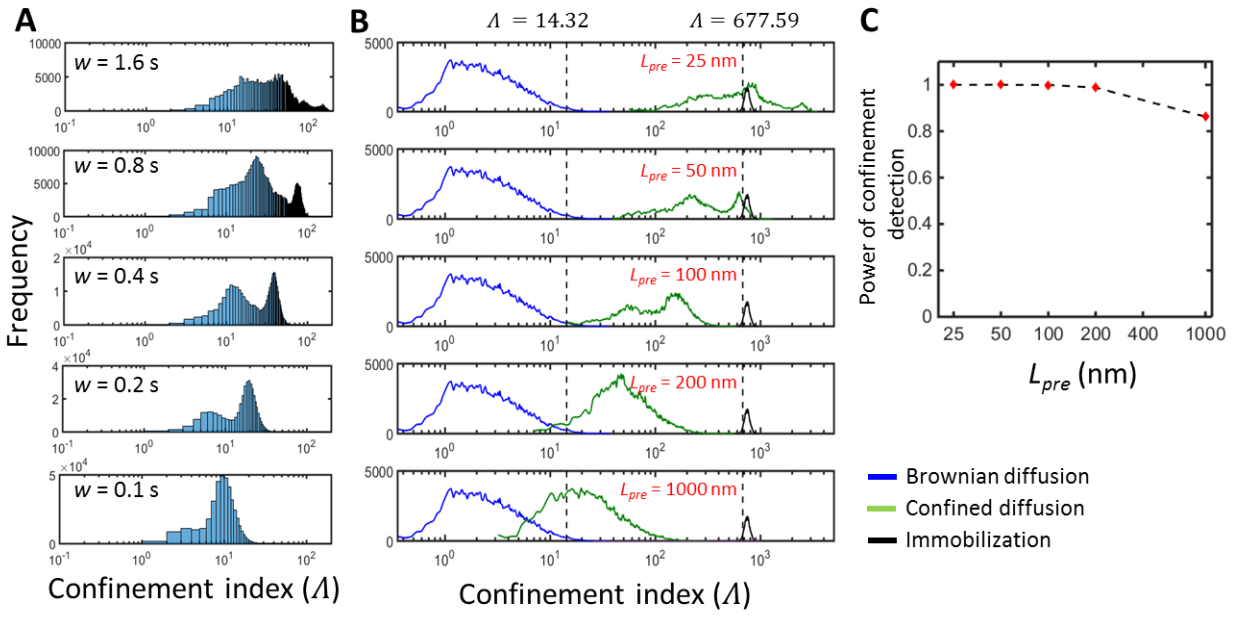

Figure S5 | Selecting thresholds of the confinement index Λ for confinement detection (Monte Carlo simulation results)

(A) The confinement index of Brownian motion is independent of the rolling window length (w) (15), but the confined index (Λ) of confined diffusion is a function of the rolling window length. **(B)** Histograms of confinement indices of freely diffusing particles (D_{Brn} = 0.08 μm^2/s, blue lines), particles diffusing within confinements of different sizes ($D_{micro,pre}$ = 0.08 μm^2/s and L_{pre} = 25, 50, 100, 200, and 1000 nm, green lines) and immobilized particles ($D = D_{min} = 4\times10^{-4}$ μm^2/s, black lines). In this simulation, we created diffusion confinements of various linear dimensions (L_{pre} = 25, 50, 100, 200, and 1000 nm) and penetrable boundary conditions (which mimic actin-cytoskeleton associated barriers and anchors). The particle can freely diffuse within the confinement ($D_{micro,\text{pre}}$ = 0.08 μm^2/s), with a probability of penetration P = 0.01 at the boundaries. We found the Λ threshod value of 14.32 can adequately differentiate confined diffusion from Brownian diffusion and the Λ threshod value of 677.59 can adequately differentiate confined diffusion from immobilization, repectively. As a result, here we define confinement diffusion to be $14.32 < \Lambda \leq 677.59$, where $\Lambda \leq 14.32$ is Brownian diffusion and $\Lambda > 677.59$ is immobilization. With this set of criteria, only 5% of simulated Brownian diffusion and immobilized trajectories were misclassified as confined diffusion. Our simulation results also indicated that the measured confinement index is a function of confinement size itself. As shown here, the set of criteria worked relatively well when the linear dimension of confinement is about 50-200 nm. The diameters of actin-induced compartments within plasma membrane range from 40 to 300 nm (5). **(C)** This plot shows that the power of distinguishing confined diffusion from Brownian diffusion. The Λ threshod value of 14.32 effectively separates confined diffusion from Brownian motion within the linear dimension of confinement (L_{pre}) below 200 nm (Power > 0.98). The statistical power is the probability that the test correctly differentiates trajectories of confined diffusion from those of Brownian diffusion.

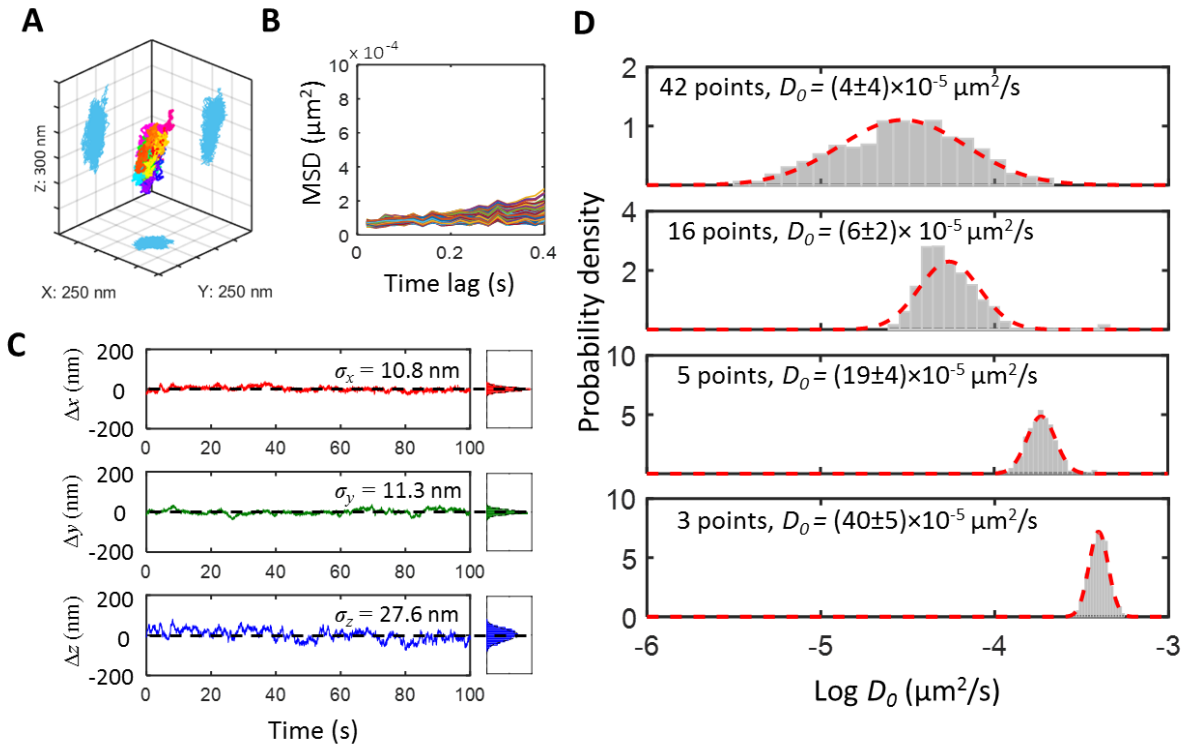

Figure S6 | Detection limit of TSUNAMI microscope (experimental tracking result)

To understand the lowest diffusion coefficient and the shortest linear dimension of confinement that TSUNAMI microscope can resolve, we performed tracking of fluorescent beads (⌀40 nm, Cat. No. F8770, Thermo Fisher Scientific) fixed in a 1.3% agarose matrix. The laser power was adjusted to achieve a photon count rate comparable to that of a real live cell tracking experiment (~400 kHz). **(A)** Representative trajectory of a bead immobilized in argarose matrix. **(B)** Segmented MSD curves using the rolling window of 1.6 s (w). The time step is 20 ms (Δt) and the sliding time step is 0.1 s (Δs). **(C)** Static tracking errors recored for x, y, and z dimesions respectively. The distances between each position (x_i, y_i, z_i) to the mean postion ($\bar{x}, \bar{y}, \bar{z}$) are Δx, Δy, and Δz. The static tracking errors, σ_x, σ_y, and σ_x, are the standard deviations of Δx, Δy, and Δz. Considering the "dynamic error" (i.e. tracking error) of the TSUNAMI microscope, the "static error" (due to the microscope thermomechanial instability) is estimated to be ~10 nm in x/y and 30 nm in z for 100-second-long experiments. **(D)** The finite values extracted from the MSD of immobilized bead represent the detection limit of the TSUNAMI system. To understand the how the number of MSD points affects the estimation of diffusion coefficients, the D_0 was estimated by fitting a MSD curve with a linear regreassion line using the first 3, 5, 16, or 42 MSD points. The number of MSD points were determined using a covariance-based estimator (19) with these following parameters: 10 nm tracking error in xy, 20 ms time step, 1.6 s tracking duration, 10^{-2}, 10^{-3}, 10^{-4}, or 10^{-5} μm²/s estimated diffusion coefficients, respectively. The D_0 converges with more MSD points, however, more MSD points also increase the variation of D_0. The number of MSD points used to estimate diffusivity of EGFRs is 3-5 points, so the lower bound of D_0 was defined as $D_0 = (19 \pm 4) \times 10^{-5}$ μm²/s using the first 5 MSD points.

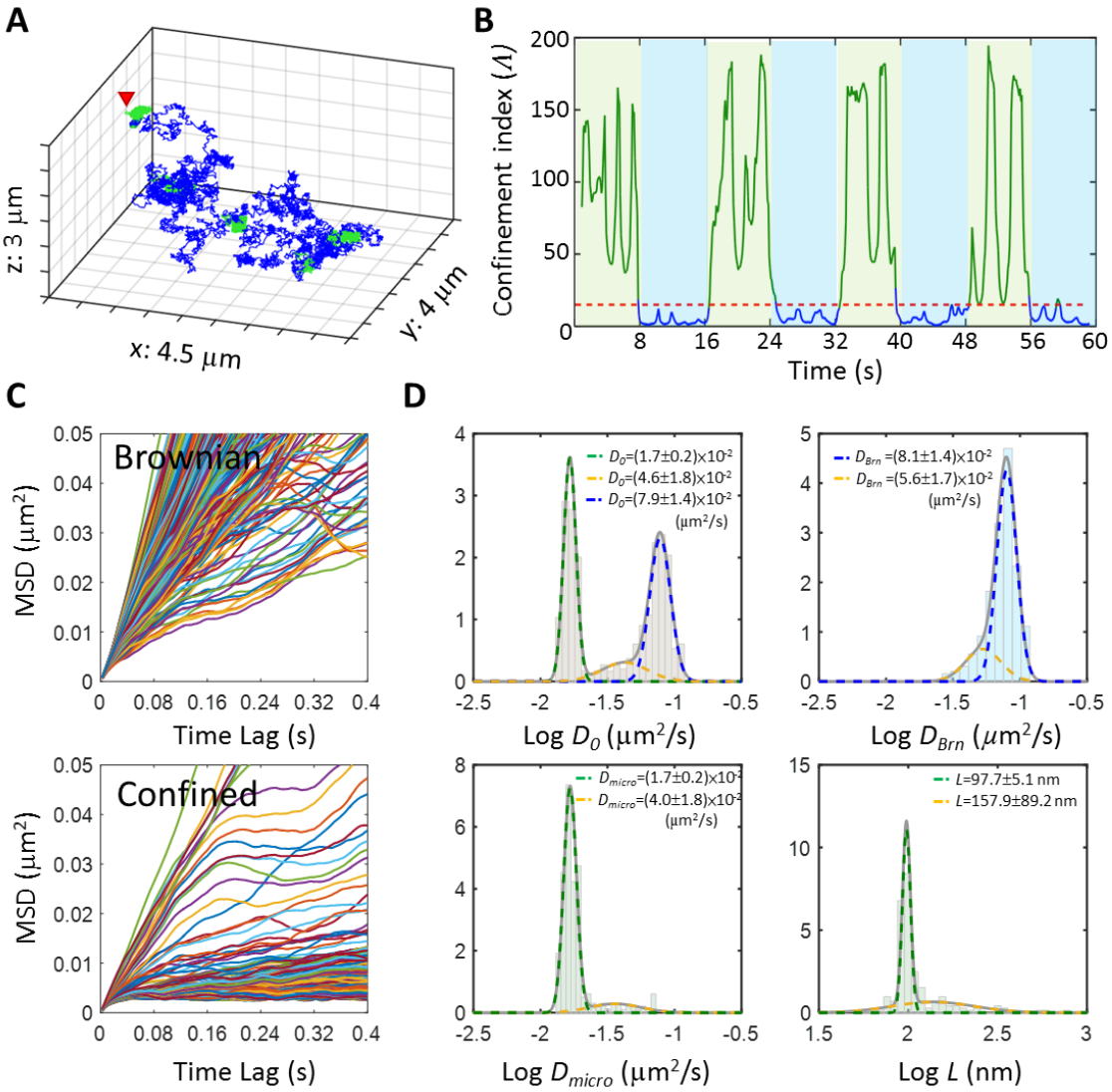

Figure S7 | Testing of MSD analysis and confinement detection (SME results)

(A) A Simulated trajectory composed of segments exhibiting Brownian diffusion and confined diffusion alternatively. Simulated condition: D_{pre} = 0.08 μm²/s, the linear dimension of confinements L_{pre} = 100 nm, probability of penetration P = 0.01 at the boundaries. The 64 s long trajectory is constituted of 8 segmemts exhibiting Brownian diffusion and confined diffusion (hop diffusion) by truns. Their motion patterns are determined by MSD analysis and confinement detection, and the trajectory are color-coded with either blue or green colors indicating Brownian diffusion and confined diffusion, respectively. The red arrow head indicates the starting point of the trajectory. **(B)** Profile of confinement index (Λ) of the trajectory. **(C)** MSD plots of segments classfied into Brownian diffusion (upper plot) or confined diffusion (lower plot). **(D)** Histograms of recovered diffusion coefficients, lengths of confined regions from Brownian diffusion (blue) or confined diffusion trajectories (green). The histograms were then fitted with a Gaussian mixture model. The fitted means and standard deviations were shown in the plots. D_{Brn} represents the recovered diffusion coefficient of Brownian trajectories. D_{micro} represents the recovered short-term diffusion coefficient of confined diffusion trajectories and D_{macro} is the recovered long-term diffusion coefficient extracted from the same trajectories. L is the recovered linear dimension of confinements.

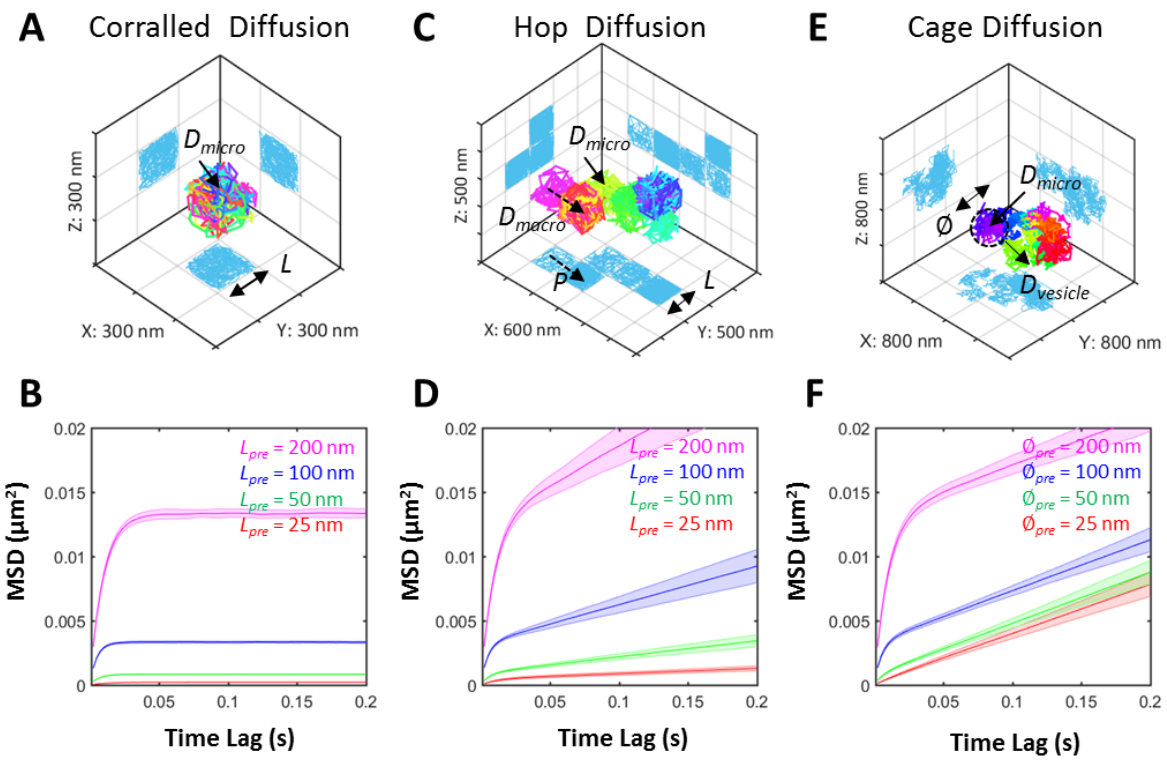

Figure S8 | MSD curves of simulation models (Monte Carlo simulation results)

MSD analysis on three types of confined diffusion models: corralled diffusion, hop diffusion and cage diffusion, which represent the possible motion patterns of EGFR trafficking. The stalled EGFRs in plasma membrane exhibits corralled diffusion (2). The hop diffusion represents the diffusion of EGFRs between membrane compartments (2, 20). The internalized EGFRs may demonstrate cage diffusion within endocytotic vesicles (13). We may be able to reveal the motion signatures of these three confined diffusion models using the MSD analysis. **(A)** Simulated corralled diffusion represents 3D isotropic diffusion in a meshwork of impenetrable barriers. **(B)** MSD plot starts linear and then reaches a plateau which identifies the confinement area and the corresponding length, L. The diffusion coefficient of this simulated confined diffusion is $D_{micro,pre}$ = 0.5 μm^2/s. **(C)** Simulated hop diffusion represents 3D isotropic diffusion in a meshwork of penetrable barriers. The prescribed length of square confinement area is L_{pre} and particles have a probability (P) of penetrating the barriers in every attempt to across barriers. **(D)** The slope of the MSD curve in long timescale is related to D_{macro}, and the meshwork constraints particle diffusion. The D_{micro} of freely diffusing particle in compartments is $D_{micro,pre}$ = 0.5 μm^2/s and the penetrating probability, P = 0.01. **(E)** Simulated cage diffusion represents freely diffusing particle ($D_{micro,pre}$ = 0.5 μm^2/s) restricted to a limited vesicle that itself can diffuse (the diffusion coefficient of the vesicle is $D_{vesicle,pre}$ = 0.01 μm^2/s and its diameter is $Ø_{pre}$ = 25 to 200 nm). **(F)** The slope of the MSD curve in short timescale is related to $D_{micro,}$ and the slope in long timescale depends on $D_{vesicle}$. Error bars (represented by color ribbons) show standard deviations of 100 runs.

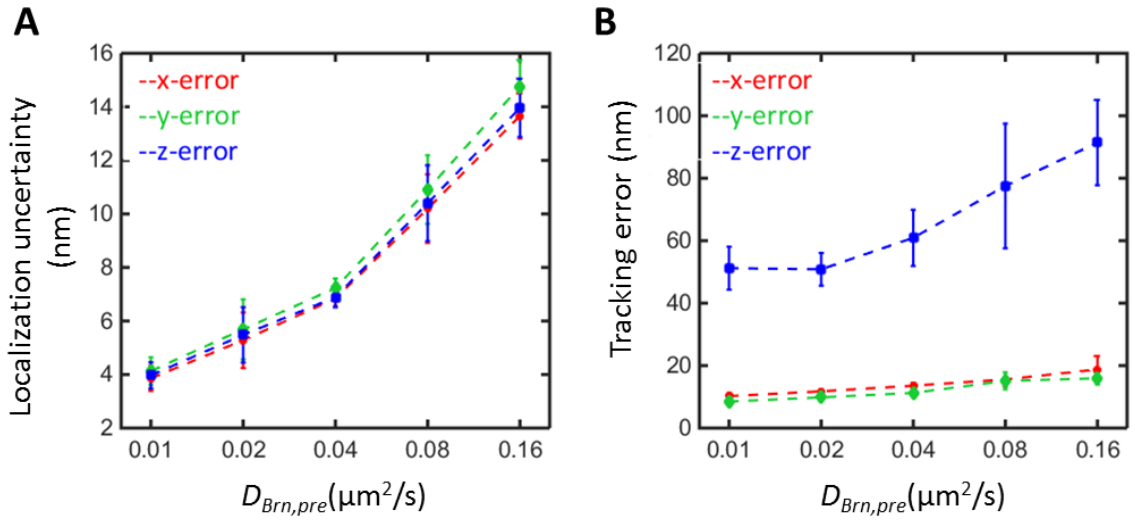

Figure S9 | Localization uncertainty of the xyz piezo stage and tracking error of TSUNAMI microscope are both related to the diffusivity of the particle (SME results)

(A) The localization uncertainty of the xyz piezo stage is defined as the standard deviation of the difference between the Monte-Carlo-simulation-generated trajectory that is used to command the movement of the xyz piezo stage and the actual trajectory that the stage performs (output from the capacitance sensors in the xyz piezo stage). The stage localization uncertainty increases with increasing diffusion coefficient in the SME. **(B)** The tracking error of TSUNAMI microscope is defined as the standard deviation of the difference between the stage trajectory (output from the capacitance sensors in the xyz piezo stage) and the TSUNAMI tracking trajectory. The tracking error was less than 20 nm in x and y and ranged from 50.8 nm to 91.4 nm in z, depending on the diffusivities used in the SME. Error bars show standard deviations of 10 runs.

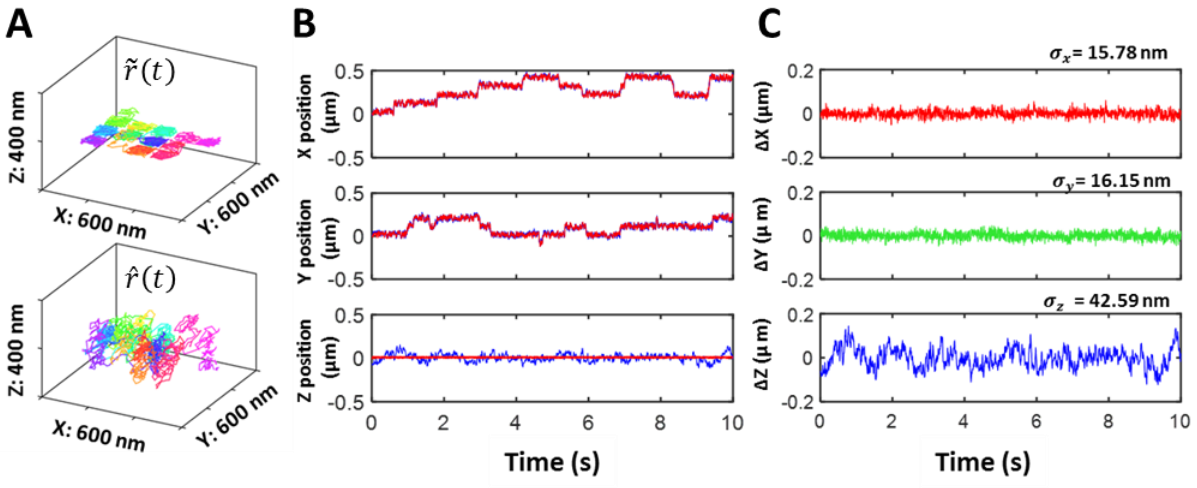

Figure S10 | TSUNAMI tracking error in 2D confined diffusion (SME results)
(A) The tracer was driven by an independent xyz piezo stage along the prescribed trajectories mimicking various motions, and the stage trajectory and the tracking trajectory were read from the piezo stage and TSUNAMI microscope. **(B)** The one-dimensional trajectories in x, y, z. The red line represents the stage trajectories and the blue ones are from tracking trajectories. **(C)** Comparing these two trajectories, the tracking errors in x, y, z directions were evaluated. The prescribed trajectory was simulated from a 2D confined diffusion model with diffusion coefficient D = 0.5 μm^2/s, probability of penetration P = 0.01 at the boundaries, and length of square compartment L = 100 nm.

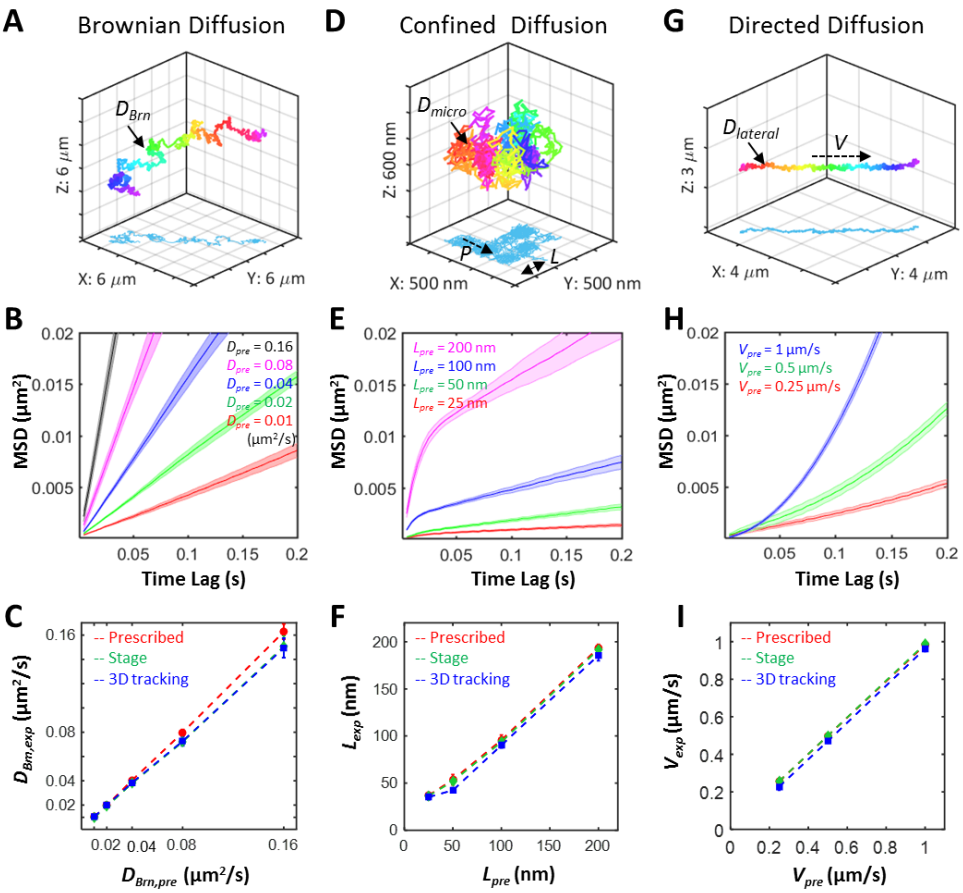

Figure S11 | MSD analysis on Brownian, confined and directed diffusion (SME results)
These SME results demonstrate that the TSUNAMI microscope is able to follow the trajectories of all three types of predefined motions (Brownian, confined, and directed diffusion), and our MSD analysis algorithm is capable of recovering the physical parameters (D_{Brn}, L and V) encoded in the prescribed trajectories. **(A)** A representative 3D tracking trajectory of Brownian diffusion with diffusivity D_{Brn} = 0.08 μm²/s. **(B)** For Brownian diffusion, the resulting MSD curves are linear with an increasing slope for larger diffusivity. **(C)** The experimental diffusivities recovered from the MSD analysis (D_{Brn}) match well with the values encoded in the prescribed trajectories (D_{pre}). R-squared values of fitted MSD curves are all above 0.99. goodness-of-fit of the fitted MSD curves was**(D)** A representative 3D tracking trajectory of confined diffusion with diffusivity D = 0.5 μm²/s in confinements of linear dimension L = 100 nm. The particle has the probability of penetration P = 0.01 at the boundaries. **(E)** For confined diffusion, the resulting MSD curves are linear initially (with a slope depends on D_{micro}) and then deviates toward a lower slope value (so-called subdiffusion). **(F)** The experimental linear dimensions of confinements recovered from the MSD analysis (L_{exp}) match well with the values encoded in the prescribed trajectories (L_{pre}). **(G)** A representative 3D tracking trajectory of directed diffusion with active transport speed V = 0.5 μm/s and lateral diffusivity $D_{lateral}$ = 0.0025 μm²/s. **(H)** For directed diffusion, the resulting MSD curves exhibit increasing slope at longer time lag (so-called superdiffusion), with the scaling exponent α = 2 for pure directed transport. Increasing lateral diffusivity in directed diffusion reduces the scaling exponent. **(I)** The experimental transport speeds recovered from the MSD analysis (V_{exp}) match well with the values encoded in the prescribed trajectories (V_{pre}). Error bars and ribbons represent standard deviations from 10 runs for each condition.

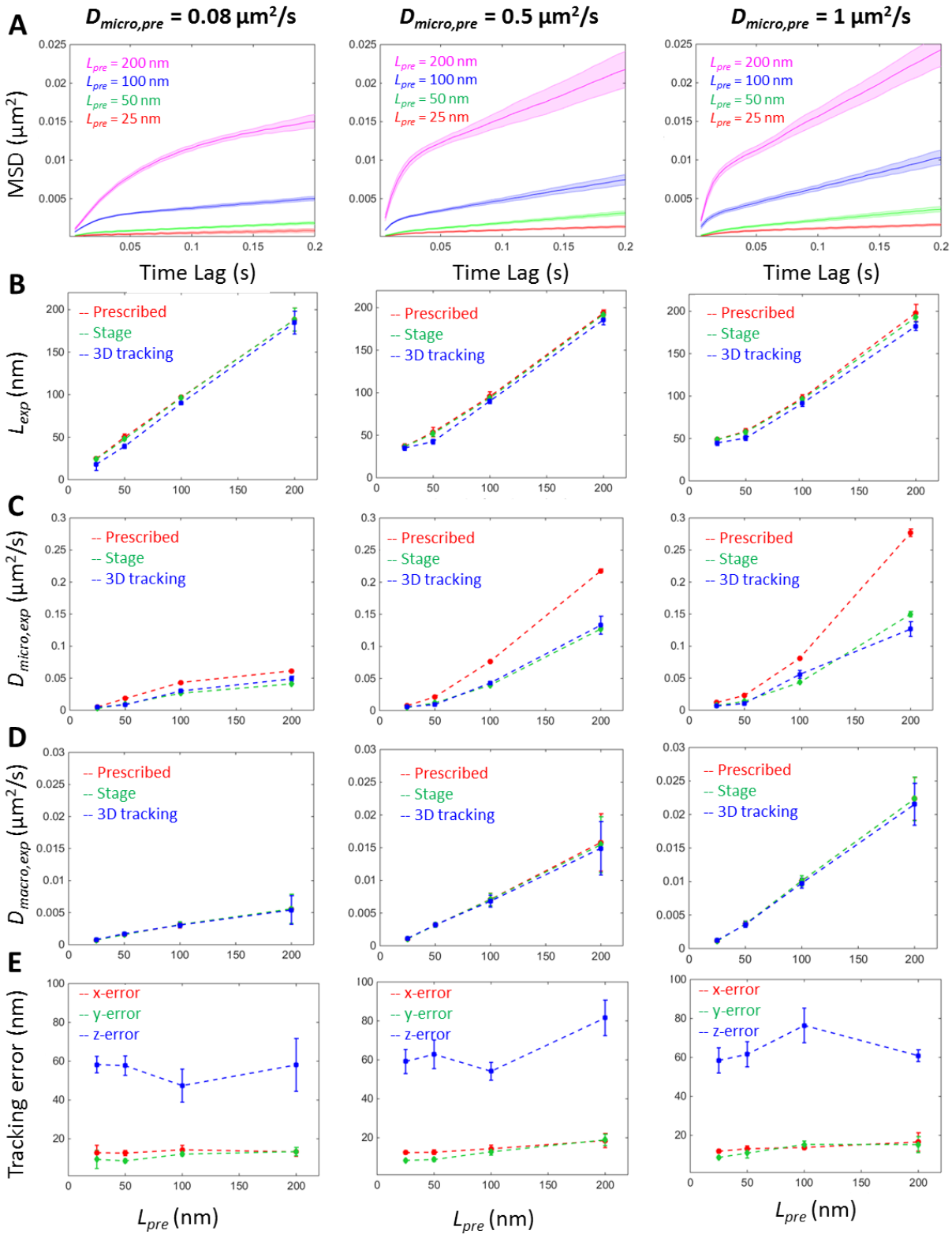
A
$D_{micro,pre}$ = 0.08 μm²/s
$D_{micro,pre}$ = 0.5 μm²/s
$D_{micro,pre}$ = 1 μm²/s
MSD (μm²)
L_{pre} = 200 nm
L_{pre} = 100 nm
L_{pre} = 50 nm
L_{pre} = 25 nm
Time Lag (s)
B
L_{exp} (nm)
-- Prescribed
-- Stage
-- 3D tracking
C
$D_{micro,exp}$ (μm²/s)
D
$D_{macro,exp}$ (μm²/s)
E
Tracking error (nm)
-- x-error
-- y-error
-- z-error
L_{pre} (nm)

F R^2 values for MSD curve fitting

D (μm²/s) \ *L* (nm)	25	50	100	200
0.08	0.738±0.117	0.957±0.007	0.994±0.004	0.995±0.008
0.5	0.908±0.024	0.979±0.007	0.999±0.001	0.998±0.001
1	0.951±0.019	0.993±0.003	0.986±0.016	0.990±0.003

Figure S12 | More MSD analysis on confined diffusion (SME results)

We further tested our MSD analysis algorithm using the confined diffusion with various D_{micro} and L values encoded in the simulated trajecotries used for SME. The particle had the probability of penetration $P = 0.01$ at the boundaries. This thorough examination further validates the reliablity of our MSD analysis algorithm in extracting encoded dynamic parameters (L and D_{micro}) and the fidelity of TSUNAMI microscope in tracking single particles under physiologically relevant conditions. **(A)** As expected, the resulting MSD curves show the signature of subdiffusion. **(B)** The experimental linear dimensions of confinements recovered from the MSD analysis (L_{exp}) match well with the values encoded in the predefined trajectories (L_{pre}) at all three diffusivities. **(C)** The short-term microscopic diffusivity, D_{micro}, obtained from the MSD analysis is influenced by the confinement size. Here we show that the short-term microscopic diffusivity D_{micro} estimated from the confined diffusion model (Equations 6 and 7) is a function of confinement size, and this finding agrees with the research of Salome's group. (21). D_{micro} is approaching the encoded value of 0.08 μm²/s only when the confinement size is sufficiently large. This result is in agreement with other research. Eggeling's group has reported that the cortical actin cytoskeleotn compartmentalised phospholipid diffusion and reduced the diffusivity of phospholipid (22). **(D)** The long-term macroscopic diffusivity, D_{macro}, obtained from the MSD analysis is also influenced by the confinement size. **(E)** Tracking error is quantified by the standard deviations of the difference between the stage trajectory (output from the capacitance sensor in the xyz piezo stage) and the TSUNAMI tracking trajectory. The tracking errors shown here are consistent with our previous observation. Error bars and ribbons represent standard deviations from 10 runs for each condition. **(F)** The goodness-of-fit of MSD curve fitting with Equation 6 (confined diffusion, in main text) was evaluated by R-squared measurment.

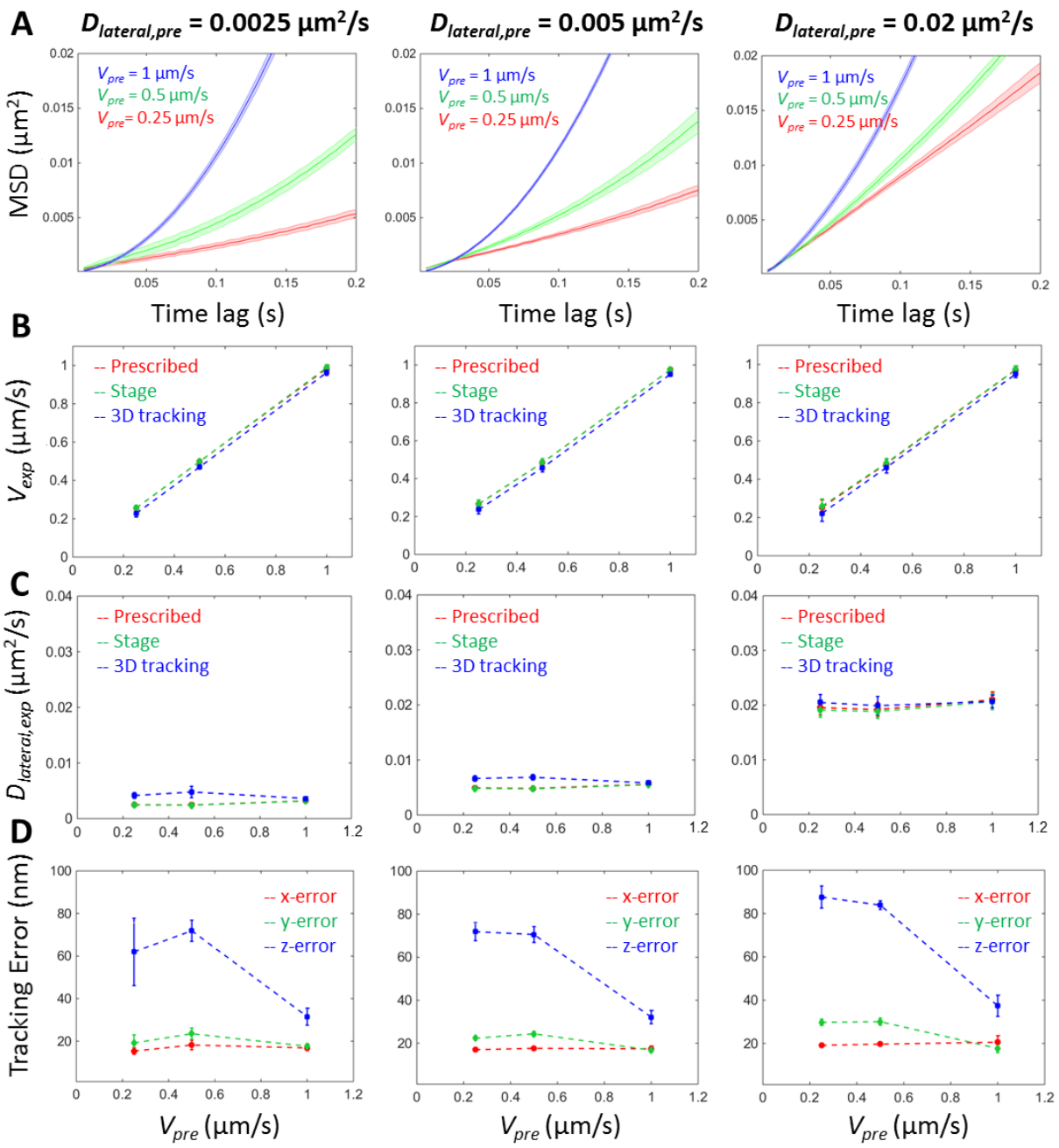

E R^2 values for MSD curve fitting

D_{Lat} (µm²/s) \ V (µm/s)	0.25	0.5	1
0.0025	0.946±0.016	0.968±0.006	0.984±0.010
0.005	0.973±0.004	0.987±0.002	0.980±0.009
0.02	0.999±0.001	0.997±0.001	0.979±0.010

Figure S13 | More MSD analysis on directed diffusion (SME results)

We further tested our MSD analysis algorithm using the directed diffusion with various D and V values encoded in the simulated trajecotries used for SME. **(A)** The MSD curves grow with time lag, exhibiting the signature of super-diffusion. The scaling exponent α is approaching 2 when the diffusivity D is vanishing. However, if D is large, the random motion would mask the directed transport. **(B)** The V_{exp} values extracted from the MSD analysis match well with the encoded V values. **(C)** The D_{exp} values extracted from the MSD analysis match well with the encoded D values at all three transport speeds. **(D)** Tracking error is quantified by the standard deviation of the difference between the stage trajectory (output from the capacitance sensor in the xyz piezo stage) and TSUNAMI tracking trajectory. The tracking error results shown here are consistent with our previous observation. Error bars and ribbons represent standard deviations from 10 runs for each condition. **(E)** The goodness-of-fit of MSD curve fitting with Equation 5 (directed diffusion, in main text) was evaluated by R-squared measurment.

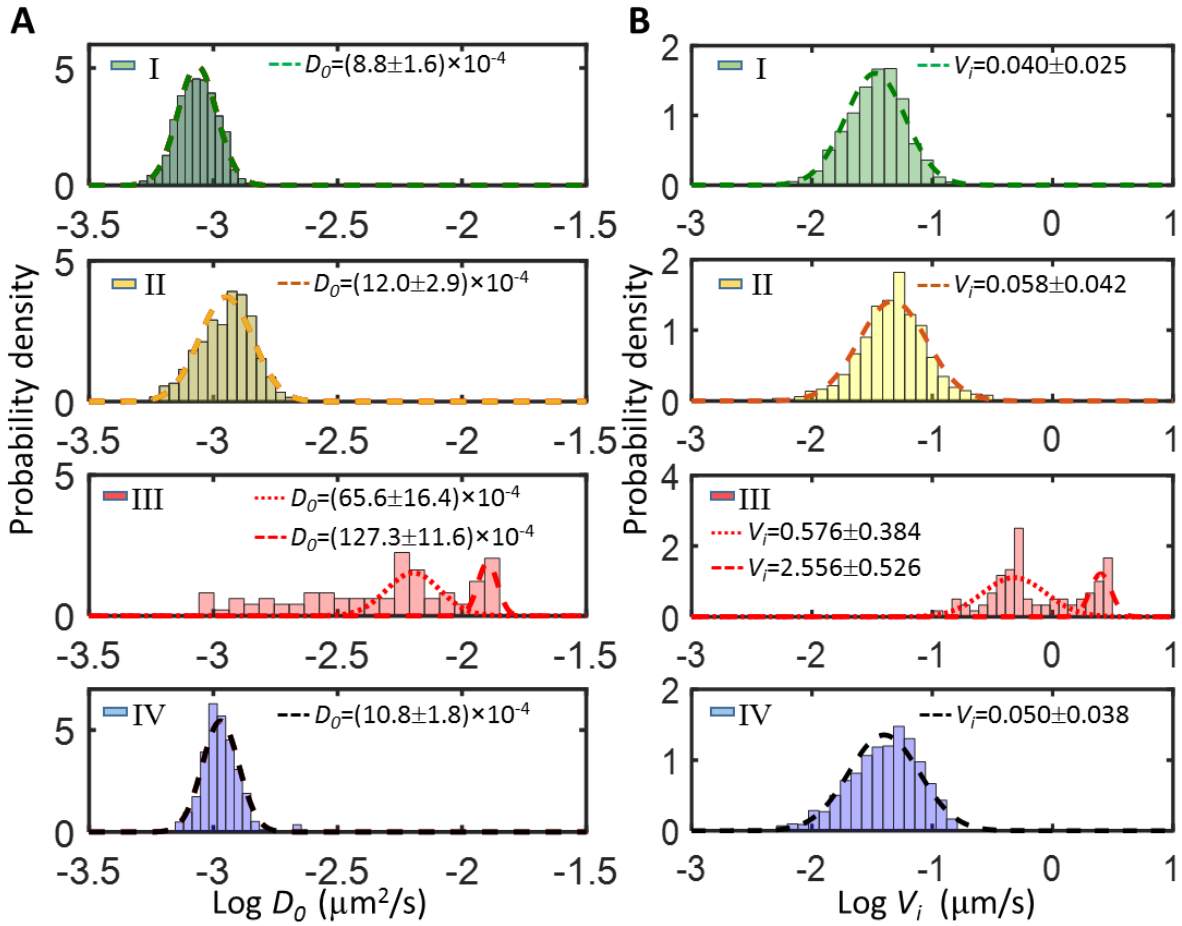

Figure S14 | Dynamic parameters of the EGFR in these four phases

Histograms of log D_o **(A)** and log V_i **(B)** in four phases of a 442-second-long trajectory (shown in Figure 5 of main text). This trajectory was dissected using the algorithm of segmentation and classification. The classified and color-coded trajectory provides a reliable guidance to identify the motional patterns of EGFRs in various phases, such as diffusion on the cell membrane, endocytosis, and active transport in cytoplasm. The dynamic parameters extracted from different phases could be used to characterized the motional features of EGFR trafficking. The diffusion coefficients (D_0) and the instantaneous velocities (V_i) recovered from the segmented trajectories of Phase III significantly differentiate from those parameters of the other three phases. As shown in the plots, the increase of instantaneous velocities is also correlated with the increase of diffusion coefficients.

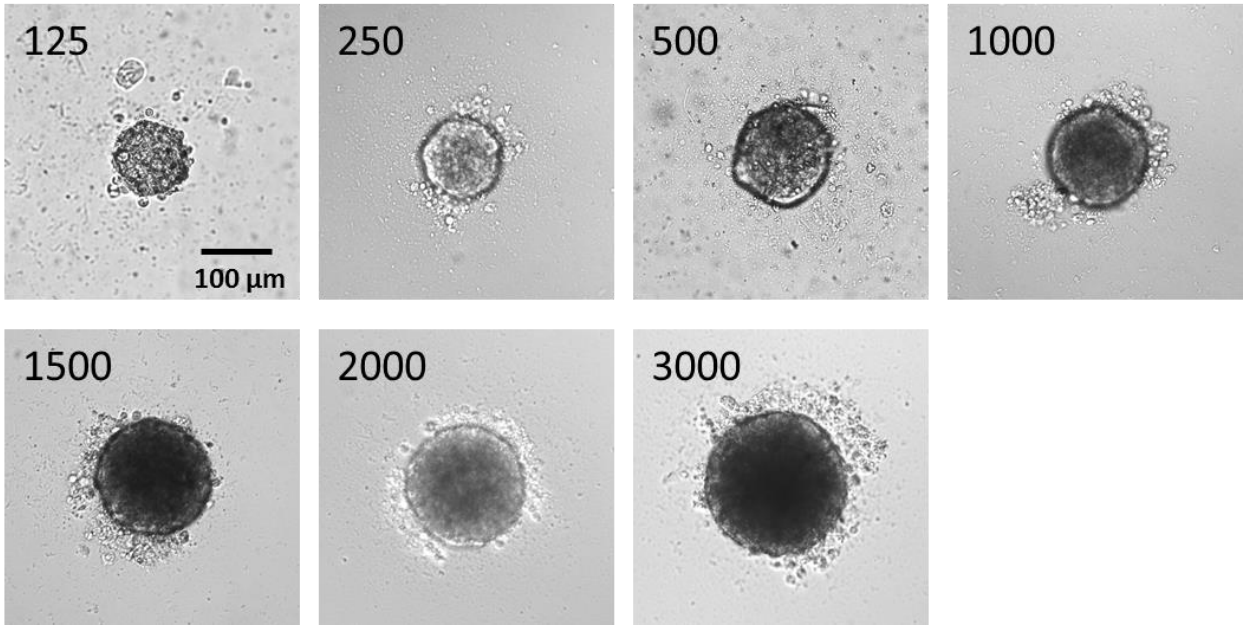

Figure S15 | Spheroid formation

Bright field imaging of multicellular cancer spheroids formed in liquid overlay from dissociated, exponentially growing A431 skin epidermoid carcinoma cells after a 96-hr initiation interval in agarose-coated 96-well microliter plates. The seeding density was between 125 and 3000 per well in 200 µl of serum-conditioned high glucose standard medium. The concentration to routinely and reproducibly obtain spheroids with a diameter of 90-110 µm is 125 cells per well. Scale bar is 100 µm. The preparation of multicellular spheroids was based on the method developed by Kunz-Schughart's group. (23)

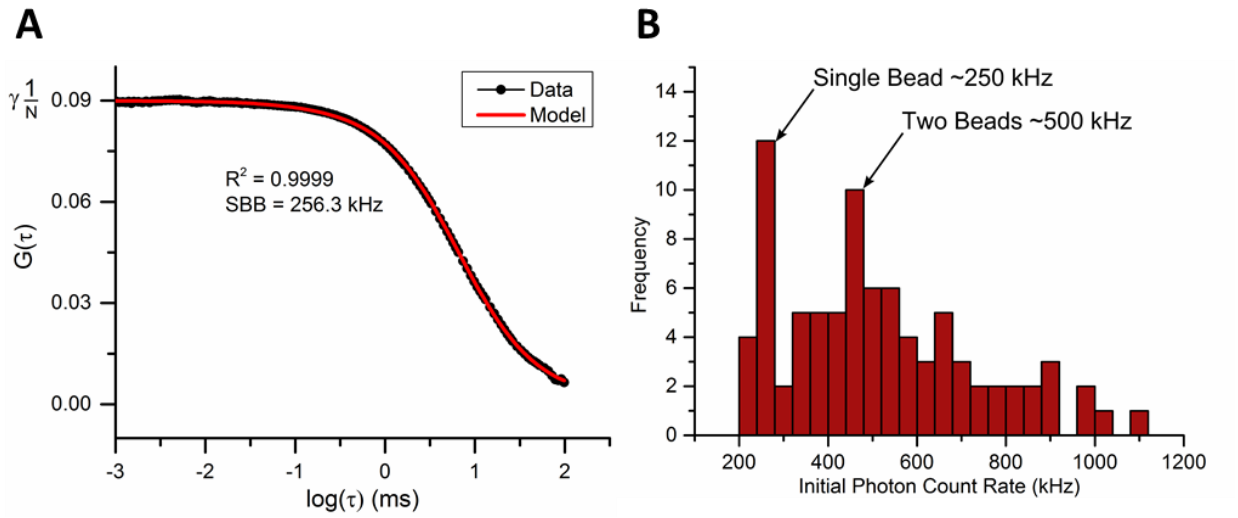

Figure S16 | Characterization of fluorescent beads for 3D tracking

(**A)** FCS Experiments and (**B)** TSUNAMI tracking trajectory analysis were used to characterize the single -bead brightness (SBB) and to estimate the number of beads attached to EGFR molecules during live cell experiments. FCS was performed with ⌀40 nm fluorescent microspheres (F8770, Thermo Fisher Scientific) in 16 nM concentration with a single excitation beam at 3 mW average power. Laser power and detector gain settings were matched to live cell experimental conditions. Raw photon counts were auto-correlated in real-time using a digital correlator (7002/USB, ALV). Autocorrelation curves (black dots) were averaged from 20 runs of 10 seconds each. Further verification of SBB is done by analyzing 95 individual trajectories' count rates. **(B)** Histogram of trajectory count rates at early time points in a fixed sample of ⌀40 nm fluorescent beads suspended in agarose. The initial count rate was taken to be the first 5 seconds of the trajectory after the controller had stably locked onto the particle (~100 ms). The histogram uncovers two peaks of brightness surrounded by a wide distribution ranging from 200 kHz to 1.1 MHz. The first peak is most likely the single bead brightness of 255 kHz whereas the second peak, at ~500 kHz, is likely a dimer. In our experiments, we made sure that we were following a single bead, not a two-bead system. This characterization has been done and published in *Nature Communications* (17), and more detailed discussion please see the supplementary information of the *Nature Communications* article.

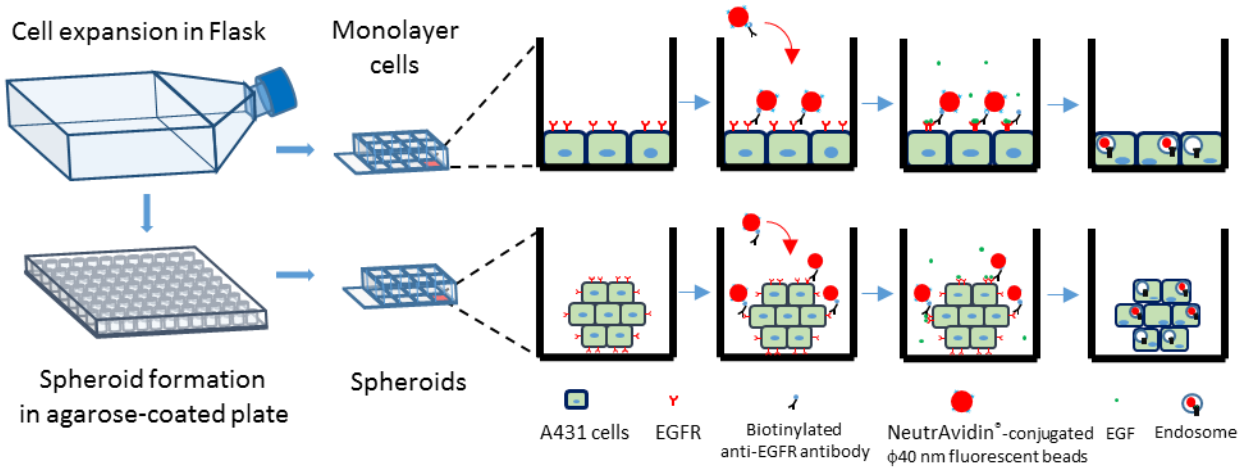

Figure S17 | Preparation of samples for EGFR tracking

A431 cells were expanded in flasks and the dissociated into single-cell suspension with trypsin treatment. For EGFR tracking on monolayer cells, the cells from suspension were directly seeded into chambered coverglasses and incubated for 24-48 hr. After 24-hr serum starvation, the monolayer cells were stained with CellMask™ Deep Red and their EGFRs were recognized by monoclonal anti-EGFR IgG conjugated ϕ 40 nm fluorescent nanoparticles. For spheroids, the suspended single cells were seeded into agarose-coated and incubated for 96 hours to form spheroids. Both monolayer cells and spheroids were treated with serum starvation 24 hour before EGFR tracking. The spheroids were then transferred to chambered coverglasses for membrane staining and EGFR labeling.

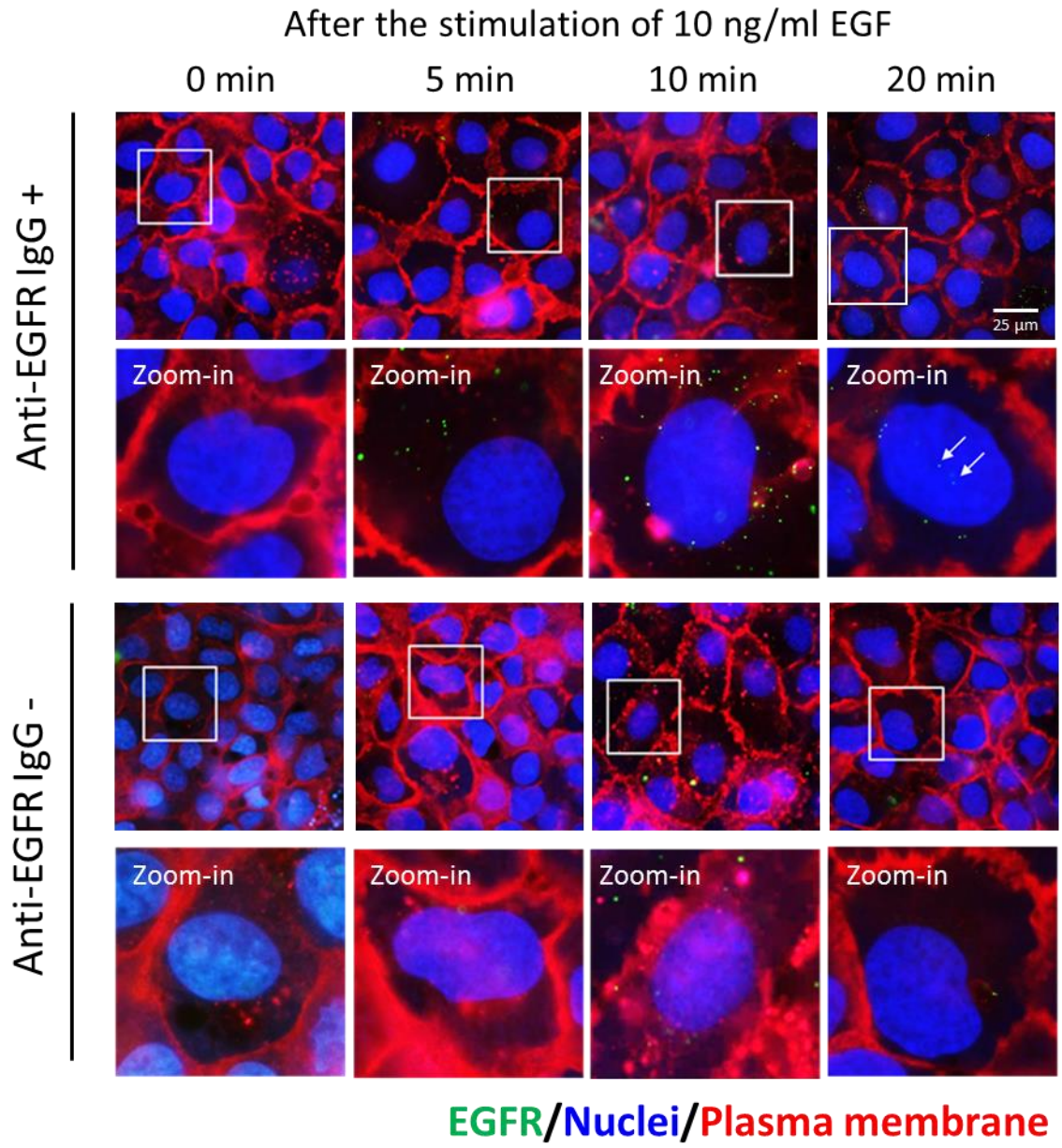

Figure S18 | EGF induces internalization of EGFR

Monolayer A431 cells were exposed to serum-free media overnight, and then their EGFRs were tagged with biotin-conjugated anti-EGFR antibodies, and NeutrAvidin® conjugated red FluoSpheres® (F8770, Thermo Fisher Scientific) bound to biotins to label EGFRs. In control group, we didn't label EGFR with anti-EGFR antibodies. After labeling, cells were treated with EGF (10 ng/ml) for indicated time. The white arrows indicate nuclear translocation of EGFR. The boxed areas are shown in detail in the zoom-in. Scale bar is 25 μm.

Supplementary References

1. Low-Nam, S. T., K. A. Lidke, P. J. Cutler, R. C. Roovers, P. M. v. B. en Henegouwen, B. S. Wilson, and D. S. Lidke. 2011. ErbB1 dimerization is promoted by domain co-confinement and stabilized by ligand binding. Nature structural & molecular biology 18:1244-1249.
2. Clausen, M. P., and B. C. Lagerholm. 2013. Visualization of plasma membrane compartmentalization by high-speed quantum dot tracking. Nano letters 13:2332-2337.
3. Kusumi, A., Y. Sako, and M. Yamamoto. 1993. Confined lateral diffusion of membrane receptors as studied by single particle tracking (nanovid microscopy). Effects of calcium-induced differentiation in cultured epithelial cells. Biophysical journal 65:2021-2040.
4. Morone, N., T. Fujiwara, K. Murase, R. S. Kasai, H. Ike, S. Yuasa, J. Usukura, and A. Kusumi. 2006. Three-dimensional reconstruction of the membrane skeleton at the plasma membrane interface by electron tomography. The Journal of cell biology 174:851-862.
5. Kusumi, A., T. A. Tsunoyama, K. M. Hirosawa, R. S. Kasai, and T. K. Fujiwara. 2014. Tracking single molecules at work in living cells. Nature chemical biology 10:524-532.
6. de Bruin, K., N. Ruthardt, K. von Gersdorff, R. Bausinger, E. Wagner, M. Ogris, and C. Bräuchle. 2007. Cellular dynamics of EGF receptor–targeted synthetic viruses. Molecular Therapy 15:1297-1305.
7. Ruthardt, N., D. C. Lamb, and C. Bräuchle. 2011. Single-particle tracking as a quantitative microscopy-based approach to unravel cell entry mechanisms of viruses and pharmaceutical nanoparticles. Molecular Therapy 19:1199-1211.
8. Fakhri, N., A. D. Wessel, C. Willms, M. Pasquali, D. R. Klopfenstein, F. C. MacKintosh, and C. F. Schmidt. 2014. High-resolution mapping of intracellular fluctuations using carbon nanotubes. Science 344:1031-1035.
9. Saxton, M. J. 1997. Single-particle tracking: the distribution of diffusion coefficients. Biophysical journal 72:1744.
10. Wade, W. F., J. H. Freed, and M. Edidin. 1989. Translational Diffusion of Class-Ii Major Histocompatibility Complex-Molecules Is Constrained by Their Cytoplasmic Domains. Journal of Cell Biology 109:3325-3331.
11. Burmaster, D. E., and D. A. Hull. 1997. Using Lognormal distributions and Lognormal probability plots in probabilistic risk assessments. Hum Ecol Risk Assess 3:235-255.
12. Lin, C., M. Schuster, S. C. Guimaraes, P. Ashwin, M. Schrader, J. Metz, C. Hacker, S. J. Gurr, and G. Steinberg. 2016. Active diffusion and microtubule-based transport oppose myosin forces to position organelles in cells. Nature communications 7.
13. Huet, S., E. Karatekin, V. S. Tran, I. Fanget, S. Cribier, and J.-P. Henry. 2006. Analysis of transient behavior in complex trajectories: application to secretory vesicle dynamics. Biophysical journal 91:3542-3559.
14. Jin, H., D. A. Heller, and M. S. Strano. 2008. Single-particle tracking of endocytosis and exocytosis of single-walled carbon nanotubes in NIH-3T3 cells. Nano Letters 8:1577-1585.
15. Meilhac, N., L. Le Guyader, L. Salome, and N. Destainville. 2006. Detection of confinement and jumps in single-molecule membrane trajectories. Physical Review E 73:011915.
16. Sergé, A., N. Bertaux, H. Rigneault, and D. Marguet. 2008. Dynamic multiple-target tracing to probe spatiotemporal cartography of cell membranes. Nature methods 5:687-694.
17. Perillo, E. P., Y.-L. Liu, K. Huynh, C. Liu, C.-K. Chou, M.-C. Hung, H.-C. Yeh, and A. K. Dunn. 2015. Deep and high-resolution three-dimensional tracking of single particles using nonlinear and multiplexed illumination. Nature communications 6.
18. Liu, C., Y.-L. Liu, E. Perillo, N. Jiang, A. Dunn, and H.-C. Yeh. 2015. Improving z-tracking accuracy in the two-photon single-particle tracking microscope. Applied physics letters 107:153701.

19. Vestergaard, C. L., P. C. Blainey, and H. Flyvbjerg. 2014. Optimal estimation of diffusion coefficients from single-particle trajectories. Physical Review E 89.
20. Clausen, M. P., E. C. Arnspang, B. Ballou, J. E. Bear, and B. C. Lagerholm. 2014. Simultaneous multi-species tracking in live cells with quantum dot conjugates. PloS one 9:e97671.
21. Daumas, F., N. Destainville, C. Millot, A. Lopez, D. Dean, and L. Salome. 2003. Confined diffusion without fences of a G-protein-coupled receptor as revealed by single particle tracking. Biophysical Journal 84:356-366.
22. Andrade, D. M., M. P. Clausen, J. Keller, V. Mueller, C. Wu, J. E. Bear, S. W. Hell, B. C. Lagerholm, and C. Eggeling. 2015. Cortical actin networks induce spatio-temporal confinement of phospholipids in the plasma membrane–a minimally invasive investigation by STED-FCS. Scientific reports 5.
23. Friedrich, J., C. Seidel, R. Ebner, and L. A. Kunz-Schughart. 2009. Spheroid-based drug screen: considerations and practical approach. Nature protocols 4:309-324.